

# Identification of jets with muons in the Tile calorimeter

T. Davídek  
Charles University, Prague

## Abstract

The identification of b-jets is important for large spectrum of physics processes, which will be studied in the ATLAS experiment. The ability of the Tile calorimeter to identify a muon inside a jet was studied. The results presented in this note are based on the combined electromagnetic (LAr) and hadronic (Tilecal) calorimeter test beam data obtained in 1996. The implications for the LVL1 trigger are discussed as well.

## 1 Introduction

The identification of a b-quark in an event (b-tagging) plays an important role in triggering the physics processes of interest. There are two main signatures of a b-jet, which can be searched for in the detector:

- identification of the secondary vertex
- a lepton, in particular muon contained in a jet

The second method is based on the fact that B-meson decays to muon with probability of  $\approx 20\%$ .

As the muon energy losses are dominated by the ionization process in the large range of its energy (up to 100 GeV in iron), muons deposit small signal in the calorimeter (compared to the showering particles in jets) but penetrate large depths. Therefore the last longitudinal sampling of the Tile hadronic calorimeter could be exploit to identify a muon, both isolated or contained in a jet (e.g. b-jet). The latter case is investigated here using real data from the test beam.

## 2 Test Beam Setup

The combined LAr+Tilecal test beam setup is described in [1]. During this test beam period, particles entered the LAr prototype at the fixed angle 12 deg, which corresponds to ATLAS  $\eta = 0.2$ .

Data sets of electrons (20, 40, 50, 80, 100, 150 and 287.5 GeV) and negative pions (10, 20, 40, 50, 80, 100, 150 and 300 GeV) were obtained during the test beam. Muons are extracted from the pion data.



The Tilecal prototype module is of a different length and segmentation than the real barrel module. Nevertheless, the material amount in front of the last Tilecal depth is approximately the same both in real ATLAS ( $7.4 \lambda_{\text{int}}$ ) and combined test beam setup ( $7.3 \lambda_{\text{int}}$  – see Fig. 1) at the pseudorapidity  $\eta = 0$ .

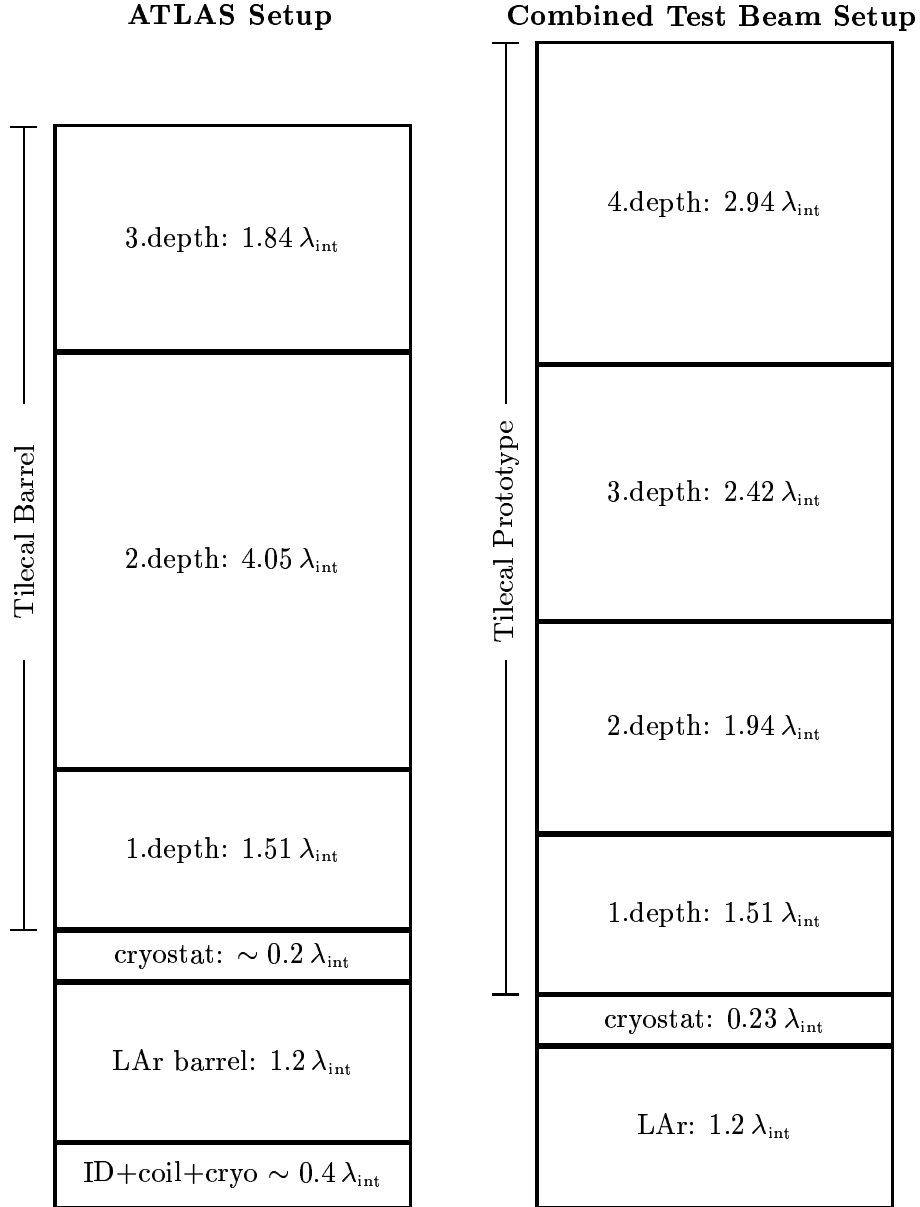


Figure 1: The material amount in front of the third Tilecal depth in the ATLAS experiment will be  $7.4 \lambda_{\text{int}}$  (at  $\eta = 0$ ). Although the segmentation of the Tilecal prototype differs from that of the real barrel Tilecal module, the material amount in front of the fourth Tilecal prototype depth in the test beam is nearly the same – it amounts to  $7.3 \lambda_{\text{int}}$ .

### 3 Procedure

In order to emulate the response of the third Tilecal sampling in ATLAS to jets, following procedure has been accommodated: first, particles are produced using Pythia and Jetset MC generator. Then all the particles are tracked in the solenoidal magnetic field, which corresponds to that in the ATLAS detector (field strength  $B = 2$  T, radius  $R = 1.15$  m). Finally, all the particles are substituted by the corresponding events from the test beam data and the response of the third Tilecal longitudinal depth is constructed.

#### 3.1 Particle Substitution

Electron or photon (coming from the MC generator) is replaced by the respective electron event from the test beam data, muon is substituted by a muon event. All the generated hadronic particles are replaced by appropriate pion events, except of those with short life-time ( $K_S^0$ ,  $\Lambda^0$  and heavier baryons). These unstable particles represent only less than 1% of all particles and are forced to decay before entering the calorimeter. Therefore they are substituted by their decay products at respective energies –  $K_S^0$  always decays to two pions and heavy baryons are replaced as they would have decayed to proton and pion.

The test beam data are available at various but discrete energies (see Section 2). The energy of the beam particle (denoted  $E_{\text{beam}}$ ) replacing the generated one (energy  $E_{\text{gen}}$ ) is chosen in the following way:

- If  $E_{\text{gen}} > E_{\text{beam}}^{\text{min}}$  (the lowest available beam energy of the respective beam particle) then the closest upper or lower beam energy to  $E_{\text{gen}}$  is taken so that the mean energies  $\langle E_{\text{beam}} \rangle$  and  $\langle E_{\text{gen}} \rangle$  of all particles of the given type ( $e^-$ ,  $e^+$ ,  $\pi^+$ ,  $\pi^-$ ,  $K^-$  etc.) are the same.
- Particles with the energy  $E_{\text{gen}} < E_{\text{beam}}^{\text{min}}$  are summed in the so-called “low-energy jets”, grouping together particles closest in space. The respective number of low-energy jets (electrons and hadrons are treated separately) is given by the formula

$$N(\text{low-E jet}) = \left\lceil \frac{\sum E_{\text{gen}}}{E_{\text{beam}}^{\text{min}}} \right\rceil + 1 \quad (1)$$

and each “low-energy jet” obeys the relation

$$E(\text{low-E jet}) \leq E_{\text{beam}}^{\text{min}} \quad (2)$$

Each such jet is then replaced by the respective beam particle at the energy  $E_{\text{beam}}^{\text{min}}$ . Since the calorimeter signal induced by one particle with energy  $E_{\text{beam}}^{\text{min}}$  is greater than that of a group of particles with the same total energy<sup>1</sup>, the hadron signal in the last Tilecal depth is slightly overestimated due to such low-energy hadrons.

---

<sup>1</sup>Example: 10 GeV pion total signal peaks at larger value than the sum of signals from two 5 GeV pions, the same is valid for the last Tilecal longitudinal sampling signals.

### 3.2 Signal in the Last Tilecal Depth

The cells sizes in the third Tilecal barrel longitudinal sampling substantially differ from those in the fourth Tilecal prototype module. Whereas the Tilecal barrel third depth cells span over  $\Delta\eta = 0.2$  (e.g. the cell D1 – centre being at  $|\eta| = 0.2$  – consists of 81 half-periods), the prototype module fourth sampling cell sizes are 22 and 24 half-periods respectively. Therefore, the signal in cell D1 is constructed as a sum of 3 (at most) appropriate prototype cells, taken into account the  $\Delta\eta$  and  $\Delta\phi$  distances of the initial generated particle direction (after the passage through the magnetic field) with respect to the beam particle direction.

The different radial size of the third sampling Tilecal barrel cells ( $1.84 \lambda_{\text{int}}$ ) and the fourth sampling prototype module cells ( $2.94 \lambda_{\text{int}}$ ) mainly causes the difference in the muon signal. Therefore, the muon signal is scaled by the factor  $1.84/2.94$  to get realistic muon response in Tilecal barrel third depth. For the other particles, the different radial size influence on the response is neglected, since the longitudinal shower profiles (both electromagnetic and hadronic) have an exponential fall-off at the large distance from the shower origin.

#### 3.2.1 Special Treatment of Low- $p_T$ Muons

A low- $p_T$  muon can be absorbed in the calorimeter either before reaching the last longitudinal sampling (thus producing no signal there) or just in the last sampling (thus depositing all its remaining kinetic energy). In order to take these effects into account, the energy losses of the generated muon are evaluated in all calorimeter longitudinal depths using the actual beam muon energy loss rescaled by the ionization energy loss ratio of the generated and beam muon:

$$\Delta E(\text{gen. } \mu) = \Delta E(\text{beam } \mu) \times \frac{dE/dx(E'(\text{gen. } \mu))}{dE/dx(E'(\text{beam } \mu))} \times \left(\frac{e}{\mu}\right)^{-1} \quad (3)$$

where  $E'(\text{gen. } \mu)$  and  $E'(\text{beam } \mu)$  stand for the actual muon energy. The electron/muon ratio

$$\frac{e}{\mu} = 0.91 \quad (4)$$

is used for evaluating the real muon energy loss in Tilecal (see [2]). The dependence of the muon signal in cell D1 on the incident muon  $p_T$  after applying the above mentioned procedure is shown in Fig. 2.

#### 3.2.2 Special Treatment of Kaons

The inelastic cross-section of kaons on protons is smaller than that of pions on protons (see Tab. 1). Since the hadronic shower longitudinal profile scales with the interaction length, the showers induced by kaons will be longer than those induced by pions.

Consequently, the number of events without the signal (i.e. compatible with noise) in the last Tilecal depth produced by incident kaons will be smaller than

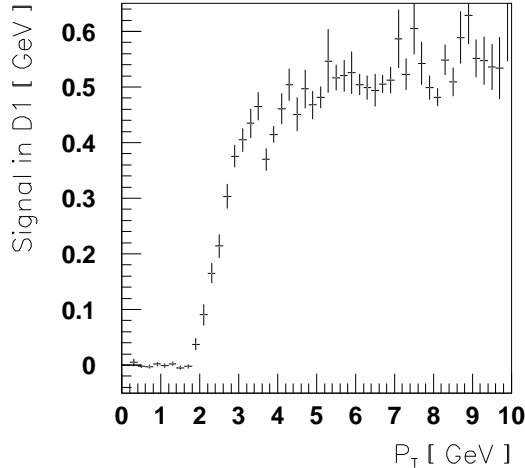


Figure 2: Muon response in the third Tilecal barrel sampling as a function of incident muon  $p_T$ . Nearly all muons with  $p_T < 2$  GeV are absorbed in calorimeter (signal consists of noise only), whereas muons above  $p_T > 6$  GeV pass through the whole calorimeter.

that from pion-induced showers. To take this effect into account, the signal in the last Tilecal depth is constructed by 1 or 2  $\pi^-$  events with the same energy. The probability of using 1 or 2 events is evaluated with help of MC simulation separately for each kaon type and incident energy. The probability of taking two pions  $P_{2\pi}$  is set so that the number of events without the signal is same both for real and simulated (i.e. constructed using pion data) kaon, e.g. for  $K^-$  the probability  $P_{2\pi}(K^-)$  obeys the relation

$$(1 - P_{2\pi}(K^-)) \times P_0(\pi^-) + P_{2\pi}(K^-) \times (P_0(\pi^-))^2 = P_0(K^-) \quad (5)$$

where  $P_0(\pi^-)$  and  $P_0(K^-)$  are the probabilities that the signal in the last Tilecal

Process	$\sigma_{\text{inelastic}}$
$\pi^- p$	22 mb
$K^- p$	19.5 mb
$K^+ p$	14 mb

Table 1: The cross-sections values concern the case when the first particle with momentum 10 GeV (laboratory frame) interact with proton [3]. The listed values illustrate the difference of the interaction length for the respective particle.

longitudinal sampling from the respective particle is compatible with the noise.

In GEANT, there are three standard hadronic packages (GEANT-Fluka, Gcalor and Gheisha), which predict different  $P_{2\pi}$ . In order to select the package best matching real data, the  $\pi^+$  and proton spectra from the Module 0 test beam data (July 1998) were compared with the MC simulation results. In the concrete, the response in the third Tilecal depth to 50 GeV protons/ $\pi^+$  at  $\eta = -0.55$  was studied.<sup>2</sup> The results are summarized in Tab. 2 – from this point of view Gcalor corresponds with data the best. In addition, the proton/ $\pi^+$  test beam spectra ratio in the third depth is compatible both with GEANT-Fluka and Gcalor prediction (see Fig. 3). Therefore, the Gcalor’s values of  $P_{2\pi}$  are used in the further analysis. Real and simulated spectrum of the  $K^-$  induced signal in the last depth is shown in Fig. 4 (note the same fraction of events compatible with noise) as well as their ratio, which is more less constant and very close to 1.

	Events without signal	
	protons	$\pi^+$
GEANT-Fluka	21 %	24 %
Gcalor	35 %	36 %
Gheisha	34 %	46 %
July 1998 data	33 %	36 %

Table 2: Number of events without the signal (i.e. compatible with noise) in the third Tilecal Module 0 depth. Comparison is shown for 50 GeV protons and pions at  $\eta = -0.55$

## 4 Results

The above described procedure is used to construct the muon as well as the jet-induced signal in cells of the third Tilecal barrel module longitudinal sampling in various processes.

### 4.1 Top–Anti-top Production

First, the process

$$p p \rightarrow t \bar{t} \rightarrow b W b W \quad (6)$$

was generated at the LHC energy (14 TeV) and events with b-jets containing a muon at  $|\eta| = 0.2$  were selected. The muon signal in the last Tilecal sampling (cell D1 for  $|\eta| = 0.2$ ) is depicted in Fig. 5 – approximately 13 % fraction is represented by soft muon, which are absorbed in the calorimeter and thus don’t contribute to the muon signal peak. As the muon is contained in the jet (and

---

<sup>2</sup>50 GeV is the lowest beam energy allowing proton/ $\pi^+$  separation using the Cerenkov counter. The last longitudinal sampling and large  $\eta$  were chosen in order to have as much material amount as possible in front ( $6.5 \lambda_{\text{int}}$ )

other jets from process (6), if sufficiently close, may contribute as well), the cell D1 total signal consists of the sum of muon and jet(s) signal (non-hatched peak in Fig. 6). The hatched area in the same figure represents the total signal without the muon contribution. The difference in these two spectra is clearly seen.

## 4.2 Inclusive Jet Production

In order to quantify the Tilecal ability to identify muons inside jets, flavour-different jets were generated at  $\eta = 0.2$  (corresponds to the test beam entrance angle) and the cell (third Tilecal barrel depth) with the highest signal is investigated. The signal of b and u-jets at 40 GeV is shown in Fig. 7 as an example. Most b-jets containing a muon give relatively high signal, so when applying the cut

$$\text{signal}(\text{cell in 3.depth}) \geq 0.25 \text{ GeV} \quad (7)$$

the efficiency of tagging the b-jet with muon (see Fig. 8) increases with energy and amounts to

$$\epsilon(\text{b-jet with } \mu) \geq 90 \% \quad (8)$$

(except of the 20 GeV jets, where the lower value of 85 % is caused by soft muons absorbed in the calorimeter). On the other hand, some non-b-jets pass this cut as well, their fraction increases with the jet energy (the u and c-jet fractions are displayed in Fig. 8 for reference). As a consequence, the rejection power against non-b-jet decreases with the jet energy (see Fig. 9). The difference between c and u-jets at lower energies is due to a part of c-jets contains a muon. Rejection power against other jets (d,s,g) coincides with that of u-jet.

## 4.3 Implications for LVL1 Trigger

The LVL1 trigger at the low LHC luminosity ( $10^{33} \text{ cm}^{-2} \text{ s}^{-1}$ ) will be set to reduce the single jet event rate to  $\sim 200 \text{ Hz}$  (see [4]). This rate will be achieved by setting the basic  $E_T$  trigger

$$E_T(\text{single jet}) > E_T^{\text{thr}} \quad (9)$$

at  $E_T^{\text{thr}} = 180 \text{ GeV}$  (see also [5]).

A suitable combination of the  $E_T$  trigger (9) and the cut (7) can result in the lower  $E_T^{\text{thr}}$  value, while keeping the inclusive jet event rate the same. The estimated trigger rates of the combined trigger

$$\left( E_T(\text{inclusive jet}) > E_T^{\text{thr}} \right) \text{ AND } \left( \text{signal}(\text{cell in 3.depth}) \geq 0.25 \text{ GeV} \right) \quad (10)$$

are listed in Tab. 3, the rates of the basic trigger (9) are listed as well. Note that the listed combined trigger rates are based on the efficiency values (see Fig. 8) obtained for  $\eta = 0.2$ . Since for larger  $|\eta|$  the efficiency of the non-b-jets

$E_T^{\text{thr}}$ (GeV)	Rate (Hz)	
	Basic trigger	Combined trigger
200	100	80
190	140	110
180	200	150
170	300	210

Table 3: The LVL1 estimated inclusive jet trigger rates for the basic (9) and combined trigger (10). Note that the listed combined trigger rates are based on the efficiency values obtained for  $\eta = 0.2$ , so for the whole range  $|\eta| < 3.2$  these rates will be slightly lower.

passing the cut (7) is smaller due to more material in front of the third Tilecal sampling, also these rates for the whole range  $|\eta| < 3.2$  will be slightly lower.

The multi-jet triggers for low luminosity are proposed  $E_T > 75$  GeV for three and  $E_T > 55$  GeV for four jets respectively (see [5]). Since the fraction of non-b-jets passing the cut (7) drops with decreasing energy (see Fig. 8), the  $E_T^{\text{thr}}$  threshold in the multi-jet event combined trigger (10) can be reduced more significantly than in case of inclusive jet trigger, still keeping the desired event rate. The combined trigger with lower  $E_T^{\text{thr}}$  will be more sensitive to the b-jets containing a muon.

## 5 Conclusion

The response of the third Tilecal barrel longitudinal depth to jets with muons was studied using the test beam data. The application of the cut (7) to the signal from the third depth cells results in the efficiency of tagging a b-jet with muon  $\epsilon(\text{b-jet with } \mu) \geq 90\%$  for  $E_{\text{jet}} \geq 30$  GeV. The rejection factor against other jets drops with increasing energy, being  $R_f = 2$  at  $E_{\text{jet}} = 100$  GeV.

Incorporation of such a cut into LVL1 jet trigger enables to decrease the jet  $E_T$  thresholds. Setting the combined trigger (10) with  $E_T^{\text{thr}} \approx 170$  GeV at the low LHC luminosity will keep the desired inclusive jet trigger rate with more sensitivity to the b-jets with muon inside.

## Acknowledgements

I would like to thank R. Leitner for advice and usefull discussion. Financial support of Prague group by the grant project RP-4210/69/97 of the Ministry of Industry and Trade of the Czech Republic is acknowledged.

## References

- [1] M. Cokal et al.: *Analysis results of the April 1996 combined test of the LArgon and Tilecal barrel calorimeter prototypes*, ATL-TILECAL-98-168

- [2] Z. Ajaltouni et al.: *Response of the ATLAS Tile Calorimeter Prototype to Muons*, NIM A **388** (1997) 64-78
- [3] C. Caso et al.: *The European Physical Journal*, **C3** (1998) 1
- [4] ATLAS Collaboration: *The Detector Performance and Physics Technical Design Report*, CERN/LHCC 99-14
- [5] ATLAS/Trigger Performance Group: *ATLAS Trigger Performance Status Report*, CERN/LHCC 98-115

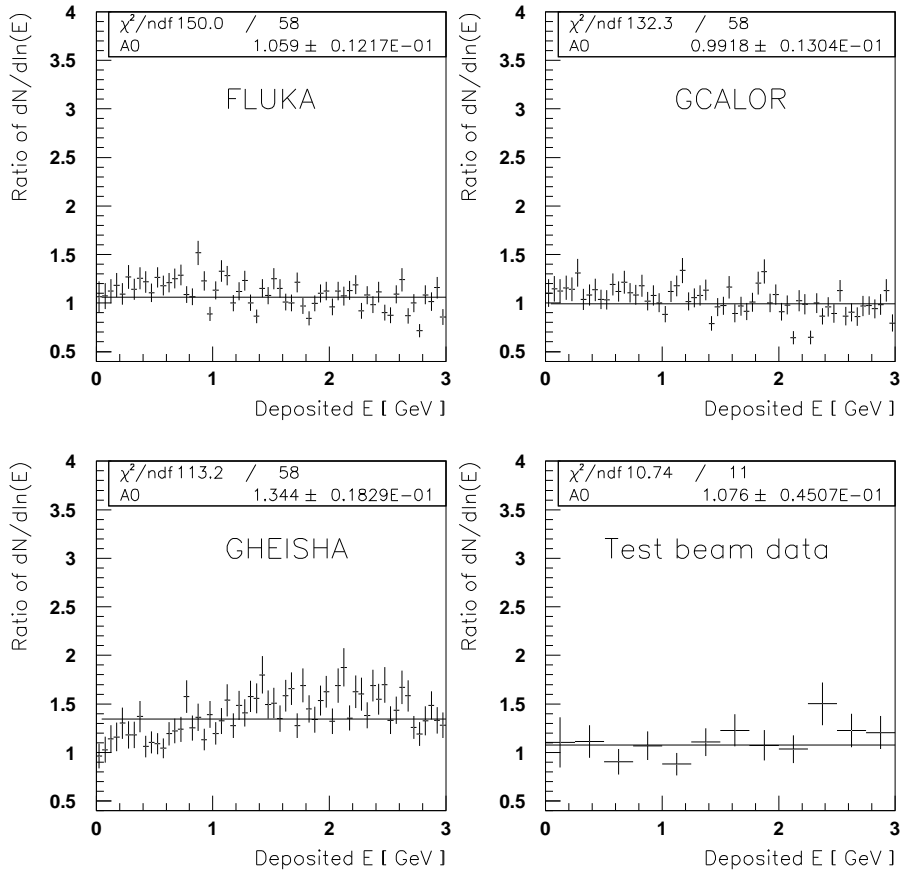


Figure 3: Ratio of proton/ $\pi^+$  spectra response in the third Tilecal Module 0 depth for the incident particle momentum 50 GeV at  $\eta = -0.55$ . The test beam results are compatible both with GEANT-Fluka and Gcalor hadronic simulation packages.

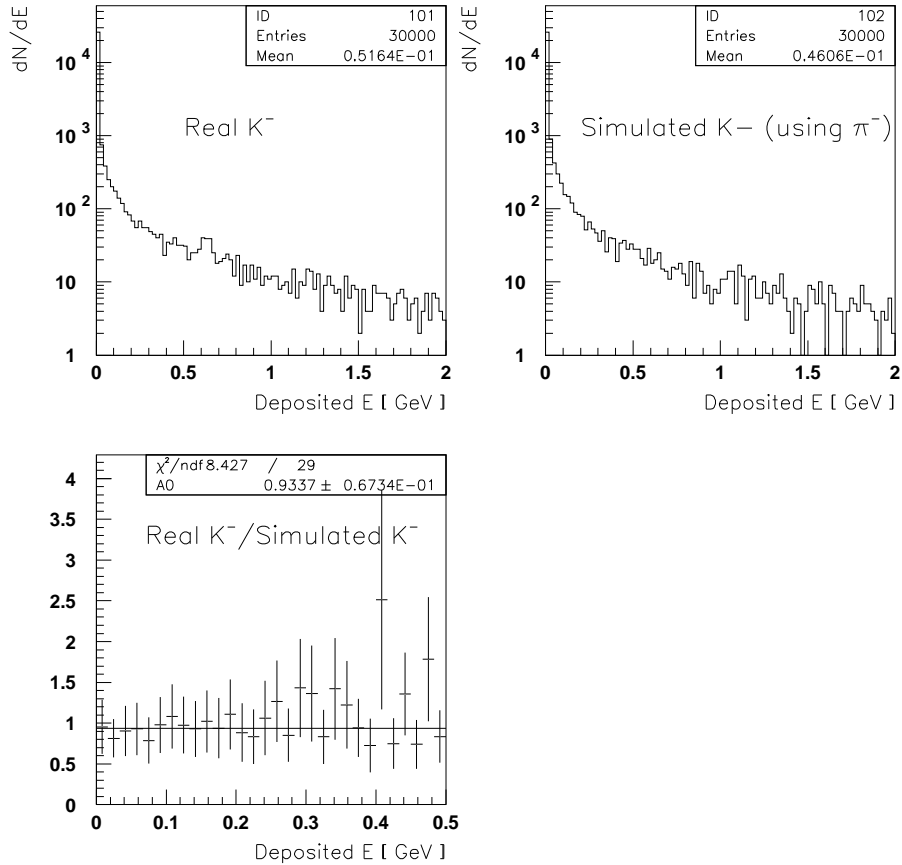


Figure 4: Energy deposited in the last Tilecal longitudinal sampling induced by incident kaons at 10 GeV with Gcalor. The spectrum of the so-called simulated  $K^-$  is obtained using 1 or 2  $\pi^-$  events with the probability given by the formula (5). Both real and simulated  $K^-$  response result thus in the same fraction of events compatible with noise and their spectra are almost the same as well (see the bottom figure, where the ratio is plotted).

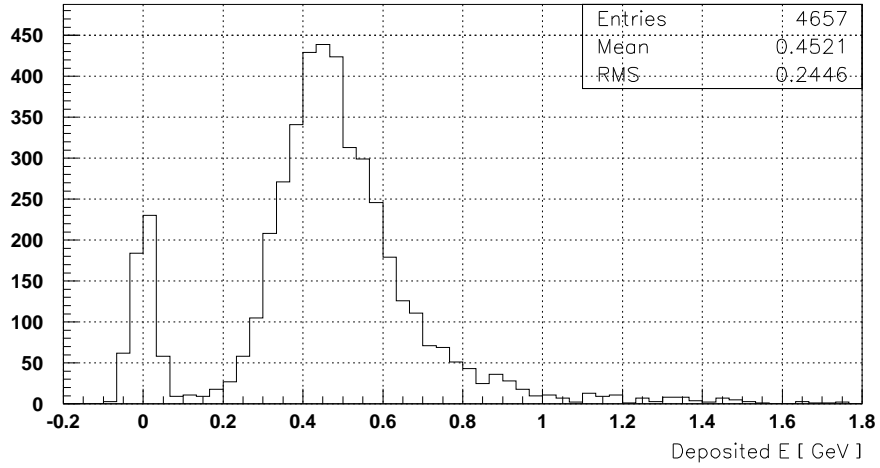


Figure 5: Signal in cell D1 from b-jet muons (process (6)). The noise peak is due to soft muons, which are absorbed in the calorimeter before reaching the last Tilecal longitudinal depth.

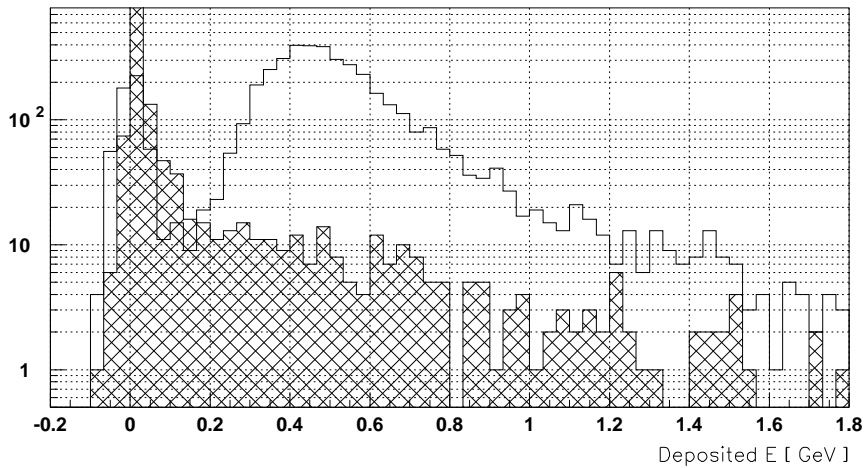


Figure 6: Total signal in cell D1, when a muon from a b-jet (process (6)) points to this cell (non-hatched peak). The hatched area represents the total signal without the muon contribution.

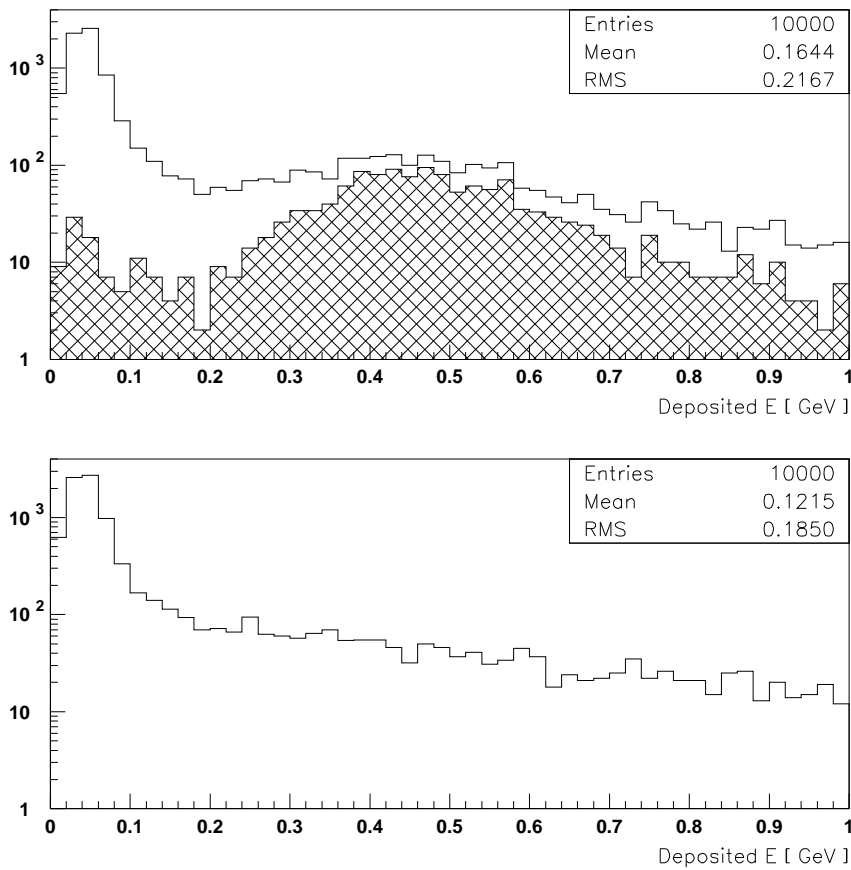


Figure 7: The distribution of the response in the third depth cell with highest signal. In the upper plot, the response to 40 GeV b-jets is shown (hatched area corresponds to b-jets with muon), whereas the lower plot represent the response to 40 GeV u-jets.

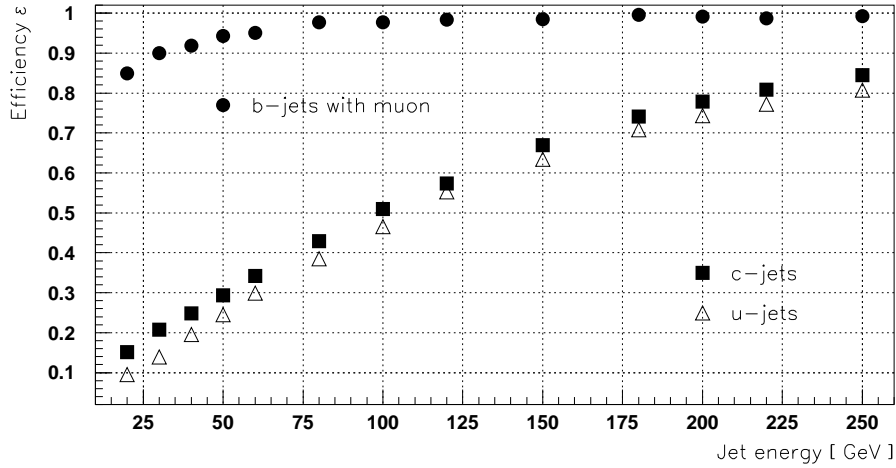


Figure 8: The efficiency  $\epsilon(\text{b-jet with } \mu)$  of tagging a b-jet with muon in the third Tilecal barrel longitudinal sampling using the cut (7). The lower value for 20 GeV jets is due to soft muons, which are absorbed in the calorimeter.

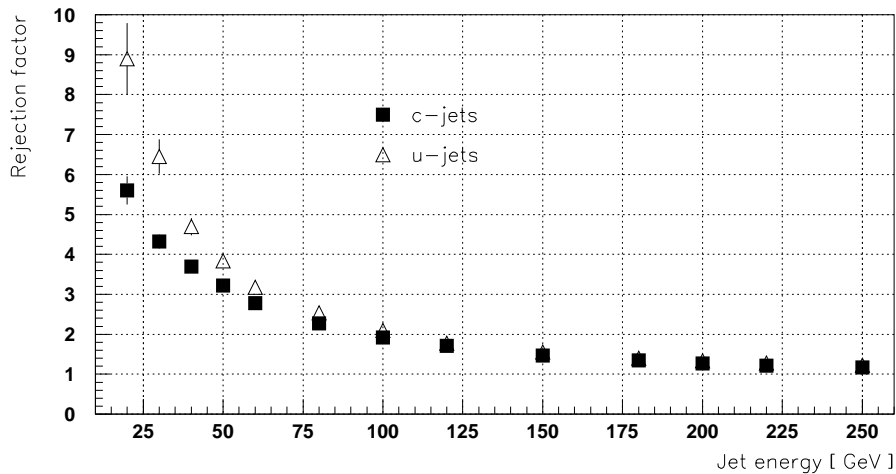


Figure 9: Rejection factor against c and u-jets using the cut (7) in the third Tilecal barrel longitudinal sampling. Rejection factor against other jets (d,s,g) coincides with that of u-jet.